Materials Advances

ROYAL SOCIETY OF CHEMISTRY

PAPER

View Article Online
View Journal | View Issue

Cite this: *Mater. Adv.*, 2025, 6, 2677

Rectification of charges on r-TiO_2 *via* Pd-cocatalysts and Schottky junctions to produce H_2 for green energy systems†

Ejaz Hussain, *[a] Muhammad Jalil,[a] Mehreen Qurban,[a] Muhammad Zeeshan Abid,[a] Muhammad Asif Khan,[b] Minhas Nazir[a] and Khezina Rafiq *[a]

For a long-term and sustainable energy system, hydrogen has been considered as one of the ideal and carbon-free fuels. A significant advantage is that it exists abundantly in the form of water, natural gas and biomass. However, the drawback is that it exists in the form of compounds and is not available in a free state. Current study was designed to produce hydrogen *via* catalytic water-splitting reactions. The advantage of the catalytic water-splitting approach is that it is an economical, controllable and more feasible technology. The efficiency of water-splitting reactions can be enhanced by various factors, such as (i) the use of more selective and effective catalysts, (ii) extending the photon absorption capability, (iii) optimizing or predicting the ideal conditions where hydrogen production rates should be maximum, (iv) controlling the charge transfer and (v) increasing the surface active sites by employing metal cocatalysts. For this purpose, stable metal oxides, such as TiO_2, were used as semiconductor supports to promote catalytic hydrogen generation. TiO_2 surfaces were tuned with Pd-cocatalysts *via* controlled hydrothermal reactions, followed by chemical reduction. Catalysts synthesized by this method were found to be more effective in term of water-splitting. The structural and optical properties of the catalysts were assessed *via* XRD, UV-Vis/DRS, SEM, TEM, AFM, Raman, FTIR, PL, and EIS analytical tools. The phase purity and elemental compositions of the catalysts were confirmed by EDX and XPS techniques. Under similar conditions, photoreactions were performed in a quartz reactor (MICQ/US-150 mL). Hydrogen evolution activities and catalytic performances revealed that the Pd/r-TiO_2 catalyst delivers almost ten times higher hydrogen (*i.e.*, 23.19 mmol g^{-1} h^{-1}) compared to pristine r-TiO_2, which delivers only 2.15 mmol g^{-1} h^{-1} of hydrogen. The higher catalytic performance of Pd/r-TiO_2 were attributed to the development of Schottky junctions that escalate and rectify the charge transfer on active sites (*i.e.*, Pd-cocatalysts). Based on the results, it is concluded that the catalysts reported herein hold potential to replace the conventional catalysts used in hydrogen generation technologies.

Received 27th December 2024,
Accepted 15th March 2025

DOI: 10.1039/d4ma01288g

rsc.li/materials-advances

Introduction

To date, fossil fuels have been the main sources of energy. Although their usage is more prominent in automobiles, conventional power sources and industries, they have several drawbacks.[1] Consumption of fossil fuels is the main source of greenhouse gas emissions. These greenhouse gases are poisonous and unacceptable to our atmosphere and healthy environment. The world is facing number of environmental issues associated with the excessive use of fossil fuels. To reduce the aforementioned problems more quickly, there is an urgent need to develop alternative fuels. Among all the alternative sources/options, the use of hydrogen is more economical and feasible for green energy technologies. Solar light and catalysts can play an important role in the transformation of chemical energy into sustainable energy (*i.e.*, hydrogen).[2] The significant advantage is that hydrogen has high energy density and can potentially replace costly and conventional fuels.[3] The use of hydrogen can significantly protect our atmosphere and fulfill energy demands, along with achieving the goal of zero emissions. Although there are many approaches to produce hydrogen, getting it from water-splitting reactions is a more reliable and cheaper option.[4]

[a] *Institute of Chemistry, Inorganic Materials Laboratory 52S, The Islamia University, Bahawalpur-63100, Pakistan. E-mail: ejaz.hussain@iub.edu.pk, khezina.rafiq@iub.edu.pk*
[b] *Department of Food Science and Technology, Faculty of Agriculture and Environment, The Islamia University, Bahawalpur-63100, Pakistan*

† Electronic supplementary information (ESI) available. See DOI: https://doi.org/10.1039/d4ma01288g

Due to excellent stability and suitable band potentials, titanium dioxide (TiO_2) has been widely used as a photocatalyst.[5] Although it appears black in mineral form, it is a white and highly crystalline solid insoluble in water. Notably, It exists in three crystalline forms, *i.e.*, rutile, anatase and brookite.[6] Among all phases, rutile TiO_2 (r-TiO_2) is most favourable due to its high chemical resistance, thermal stability, and suitable band gap (*i.e.*, 2.9 eV).[7] It can be coupled with other semiconductor systems to enhance the catalytic efficiencies. For example, the synthesis of r-TiO_2 heterojunctions with g-C_3N_4/r-TiO_2, CdS/TiO_2, MXene/TiO_2, rGO/TiO_2, and Cu_2O/TiO_2 have been found to be effective for water-splitting reactions.[8–13] Another advantage is that r-TiO_2 can be potentially tuned with metal cocatalysts (*i.e.*, Pd in the current work) in order to escalate and rectify the photoinduced charges (e^-/h^+).

As indicated in the literature, pristine r-TiO_2 is a direct band gap semiconductor, and charge recombination is relatively high due to overpotential.[14] Thus, different strategies can be utilized to reduce its overpotential. These strategies include (i) metal or non-metal doping, (ii) noble metal loading, (iii) surface modifications, (iv) alteration in band potentials, (v) formation of heterojunctions and (vi) extending the absorption capability of the photon.[15] The deposition of catalytically active metals, *i.e.*, Pt, Ni, Cu, Au, and Ag, can be successfully achieved to reduce and mimic charge recombination. Many reports have indicated that catalytic performances can be enhanced by loading metal cocatalysts, *i.e.*, Au@$Zn_3V_2O_8$, Cu@CdS, Pd@gC_3N_4, and metal-loaded $CeVO_4$.[16–18] Additionally, metal or non-metal doping can also improve catalytic performances. It has been reported that the presence of cocatalysts on r-TiO_2 lattices alter its optical and structural characteristics.[17,19]

It is worth mentioning that the presence of palladium (Pd) on the r-TiO_2 surfaces increases catalytic performances during the photoreaction. Another important factor is that the dispersion of Pd-cocatalysts on the surface is quite important for water-splitting reactions.[20,21] It has been predicted that a high dispersion of metal particles can be successfully achieved *via* the chemical reduction approach.[22] Catalysts that have been developed *via* the chemical reduction approach exhibit higher catalytic performances than those prepared by other methods.[23] Normally, r-TiO_2 absorbs UV radiation, but its absorbance is shifted to the visible region after Pd loading. It has been reported that r-TiO_2 exhibits a higher refractive index and scatters more light, promoting photon absorption.[24,25] Another significant advantage is that r-TiO_2 has excellent commercial potential due to its non-hazardous nature.

Currently, hydrogen fuel is receiving much interest as a sustainable energy source.[26] Several methods, such as thermal combustion, biomass, photocatalysis and steam reforming, can be used for hydrogen generation. However, all the aforementioned approaches have numerous drawbacks, for example, (i) less stability and photocorrosion, (ii) low quantum yield and efficiencies, (iii) relatively higher costs, (iv) excessive use of land and labour, (v) storage and transportation, and (vi) extra burden of expert engineers.[27] However, obtaining hydrogen *via* catalytic water splitting is the most suitable and reliable method to carry out the reaction on sunlight.[28] Challenges associated with water-splitting reactions can be successfully overcome by developing Schottky junctions *via* metal cocatalysts. Thus, developing the Schottky barrier at the interface, rectifies the charge transfer to the active centres (metal cocatalysts).[29,30]

In the current work, we designed Pd/r-TiO_2 catalysts (*i.e.*, having various Pd ratios on r-TiO_2), which were assessed for the hydrogen generation reactions. Results indicated that the hydrogen generation rates of Pd-loaded catalysts were quite higher than that of pristine r-TiO_2. The catalytic activities and performances are discussed in the latter section. It is found that higher activities were due to the Schottky junctions and relatively higher active sites in the case of Pd/r-TiO_2. Various factors, such as the pH, temperature, light intensity, and photocatalyst dose, affecting the hydrogen generation performances were assessed and discussed.

Experimental

Chemicals

Chemicals used in this work are listed in the ESI.†

Synthesis of photocatalysts

In the current study, r-TiO_2 was synthesized using a recently reported approach.[31] However, to produce Pd/r-TiO_2, 200 mg of r-TiO_2 was added to 40 mL of distilled water and magnetically stirred for 30 min to obtain a homogeneous slurry. To deposit the Pd-cocatalyst on r-TiO_2 surfaces, nominal amounts of the Pd precursor were used to prepare a series of photocatalysts. For this purpose, the solution precursor of palladium (Pd) was transferred to the above slurry. After 10 min sonication, metal ions were reduced using the freshly prepared cold sodium borohydride solution. The reaction mixture was stirred for 1 h and sonicated for about 20 minutes. Subsequently, the reaction mixture was transferred into the Teflon vessel, which was placed in the stainless steel autoclave reactor for hydrothermal reactions and treatments.[32] Upon completion of the hydrothermal reaction, the catalyst precipitates were collected *via* a vacuum filtration assembly. The protocol and synthesis schematic are illustrated in Fig. 1. The as-synthesized catalysts were dried directly in sunlight to evaporate/eliminate the moisture contents. A similar procedure was adapted for the synthesis of other catalysts of the series with various Pd/r-TiO_2 (*i.e.* 0.4 to 1%) metal contents on the r-TiO_2 support.

Characterization of catalysts

For the structural, optical and electrical assessment of catalysts, various advanced techniques like XRD, FTIR, Raman, TGA, SEM, EDX, AFM, XPS, PL, UV-Vis/DRS and EIS were used. The detailed descriptions of these analytical tools are given in the ESI.†

Hydrogen generation experiment

To generate hydrogen, the photoreaction was carried out in a MICQ/US-150 mL vessel and UV lamp (100 W, 360 nm) that was used as an irradiation source. About 6.5 mW cm^{-2} of photon flux, which is comparable to the UV flux in daylight, was used for

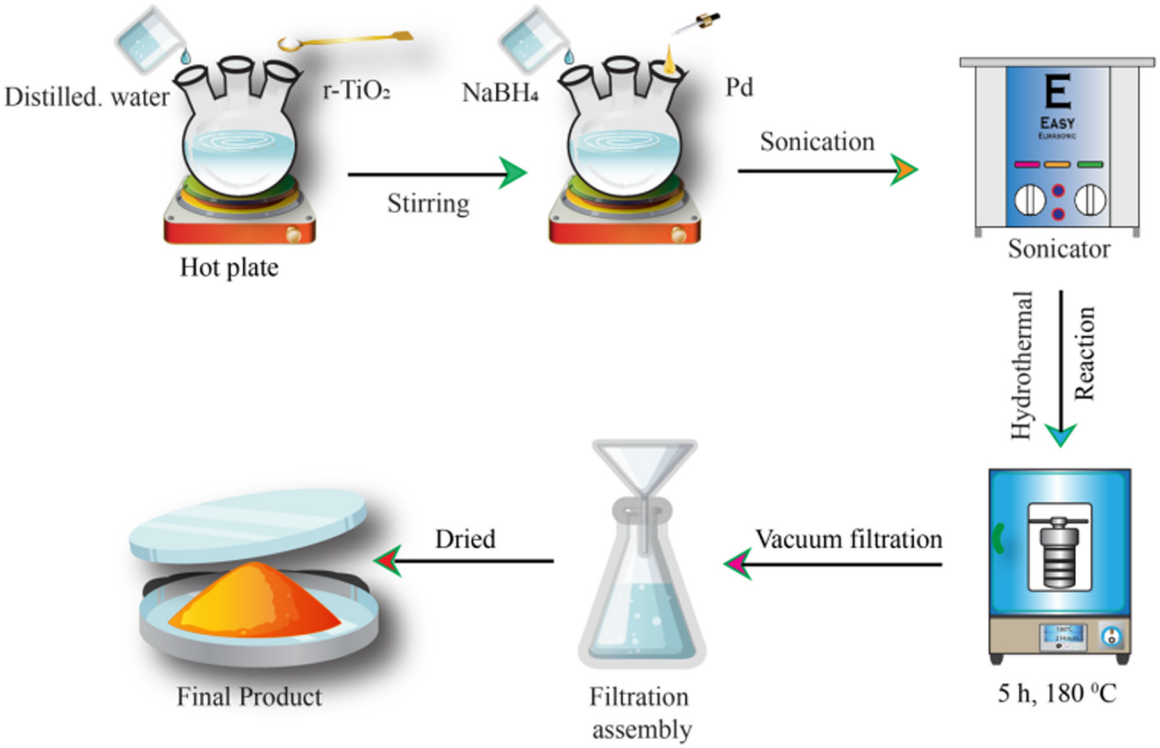

Fig. 1 Synthesis scheme for the preparation of Pd/r-TiO_2 catalysts.

exposure on reactor walls. 6 mg of the catalyst was added to 30 mL of distilled water in the reactor, along with 5% ethanol as a sacrificial reagent. In order to eliminate the dissolved oxygen contents, nitrogen gas was continuously bubbled through the reaction mixture at a flow rate of 10 mL min^{-1} for 30 minutes. To evaluate the hydrogen production, 0.5 mL of gas from the headspace of the reactor was taken at various intervals and injected into a gas chromatograph (GC-Shimadzu 2014), which was outfitted with a thermal conductivity detector (TCD). Ar gas was used as the carrier gas in the gas chromatography. The amount of H_2 generated *via* the photoreaction was measured in relation to an internal calibration curve. For each of the as-synthesized catalysts, the photocatalytic experiments were repeated thrice. The H_2 gas evolution rate was measured in both mmol g^{-1} and mmol g^{-1} h^{-1} units, allowing for a quantifiable comparison of various activities of the Pd/r-TiO_2 catalysts. The quantum efficiencies of hydrogen generation were calculated using the following equation:

$$QE = \frac{\text{Total no. of hydogen produced}}{\text{Total no. of photons consumed by catalysts}} \times 100 \quad \text{(i)}$$

Results and discussion

XRD analyses

The XRD patterns of r-TiO_2 and Pd/r-TiO_2 are shown in Fig. 2a. The results indicated that the XRD peaks appeared at the two theta (2θ) values of 27.43°, 36.07°, 41.23°, 44.04°, 54.31°, 56.62°, 62.75°, 64.04°, 69.00° and 69.80°, corresponding to the (110), (101), (111), (210), (211), (220), (002), (310), (301) and (112) crystal planes. These results prove the purity of catalysts, as per our synthesis protocol. The XRD pattern can be justified by comparing it with the JCPDS card (PDF#75-1748). The XRD patterns of Pd/r-TiO_2 remained unchanged; however, a small characteristic diffraction peak appeared at 39.18° (200), corresponding to the Pd-cocatalysts present on the r-TiO_2 surface. The JCPDS card PDF#87-0641 provides further evidence for this.[33]

Raman analyses

In the catalysts, namely r-TiO_2 and Pd/r-TiO_2, intermolecular bonding and rotational and vibrational modes were investigated using Raman spectroscopy.[34] These analyses provide valuable information on the chemical structure and composition of the material. Results indicated that TiO_2 exhibits distinct vibrational modes at 148 cm^{-1} (B_{1g}), 243 cm^{-1}, 450 cm^{-1} (E_g), and 610 cm^{-1} (A_{1g}), corresponding to the O–Ti–O vibrations in the rutile phase of TiO_2, as depicted in Fig. 2b. The 450 cm^{-1} E_g vibrational mode corresponds to the oxygen bond vibrations in O–Ti–O, whereas the vibrations at 148 cm^{-1} and 610 cm^{-1} correspond to the B_{1g} and A_{1g} symmetric and anti-symmetric vibration modes, respectively. A vibration at 243 cm^{-1} was due to the typical multiple phonon scattering.[35] It is worth mentioning that a slight shift was observed in the Raman spectrum of Pd/r-TiO_2 catalysts. This minute shift was indicated in the 610 cm^{-1} to 609 cm^{-1} range due to the presence of Pd-cocatalysts (low metal contents) on the r-TiO_2 surfaces.[36]

Fourier transform infrared (FTIR) analyses

The FTIR results of r-TiO_2 and Pd/r-TiO_2 are illustrated in Fig. 2c. The range for identification of functional groups on

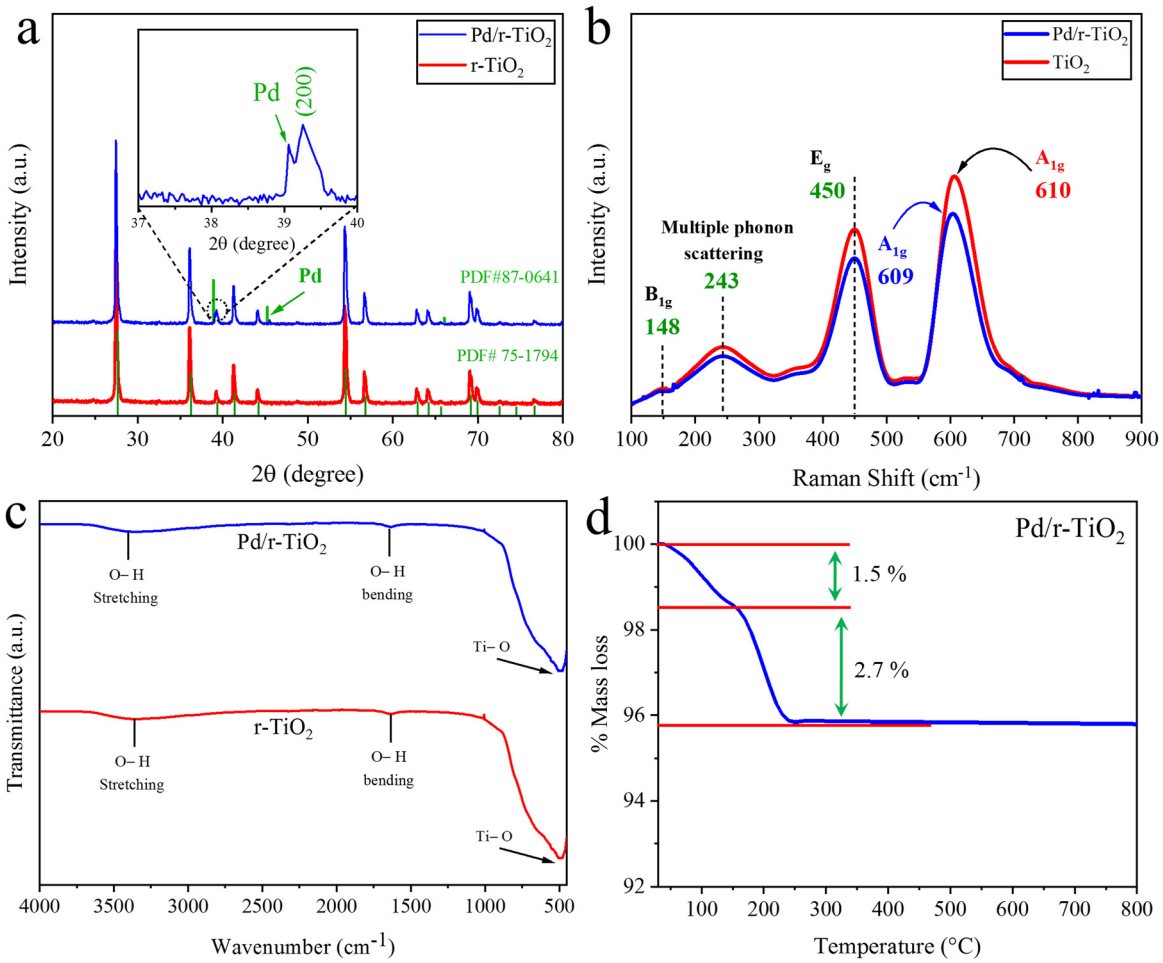

Fig. 2 (a) XRD patterns (inset: zoomed view of Pd diffraction), (b) Raman spectrum, (c) FTIR results r-TiO_2 and Pd/r-TiO_2 and (d) TGA analysis of Pd/r-TiO_2.

the catalyst is 4000 cm^{-1} to 500 cm^{-1}. In the FTIR results of Pd/r-TiO_2, no obvious change was observed due to the low metal loading. A strong peak was observed at 503 cm^{-1} due to the O–Ti bond in the r-TiO_2. Two peaks at 1600 cm^{-1} and 3400 cm^{-1} were attributed to the bending and stretching vibrations of the –OH group, respectively.[37,38] Hydroxyl groups were detected due to the presence of moisture content in the interstices of the ascribed catalysts.

Thermogravimetric analysis (TGA) assessment

Thermogravimetric analysis was conducted to ensure the catalyst stability at higher temperatures.[39] TGA calculates the sample mass changes in relation to temperature and time.[40] The thermal breakdown of catalyst particles was determined from the information provided by TGA. TGA is not suitable to directly identify the gases released from the sample when it is heated in a controlled furnace. Up to 150 °C thermal temperature, a 1.5% weight loss was attributed to the loss of water contents. Similarly, up to 240 °C, another 2.7% weight loss was due to residual oxides, as shown in Fig. 2d. After this temperature, catalysts remained stable and no further weight loss was observed even at higher temperatures. The TGA results revealed that the as-synthesized catalysts, *i.e.*, Pd/r-TiO_2, exhibit enough stability and have the potential for application under extreme conditions.

SEM and EDX analysis

SEM is a widely used technique in which an electron beam scans a sample and provides a magnified image. This technique is highly useful for the morphological studies of solid inorganic materials. Catalyst morphology has a significant influence on the performance of the catalysts for photoreactions.[41] The surface morphology of Pd/r-TiO_2 catalysts was assessed by SEM analysis, and the results are presented in Fig. 3(a) and (b). The SEM images of r-TiO_2 confirm the spherical homogeneous morphology. As indicated in Fig. 3b, at 500 nm resolution, Pd-cocatalysts were clearly observed on the r-TiO_2 surfaces. Cocatalysts (*i.e.*, Pd) at the semiconductor support interface showed that the loading of cocatalysts is successfully achieved. According to Fig. 3(a) and (b), r-TiO_2 particles have spherical morphology with uniform size and shape. The homogeneous deposition of Pd over the r-TiO_2 surface is not discernible as independent entities due to the low concentration of the metal. Furthermore, the purity and elemental composition of the as-prepared catalysts were determined by EDX analysis.[42] All essential elements of the catalysts, such as Ti, O and Pd, were detected in the EDX spectrum, as shown in Fig. 3e. The

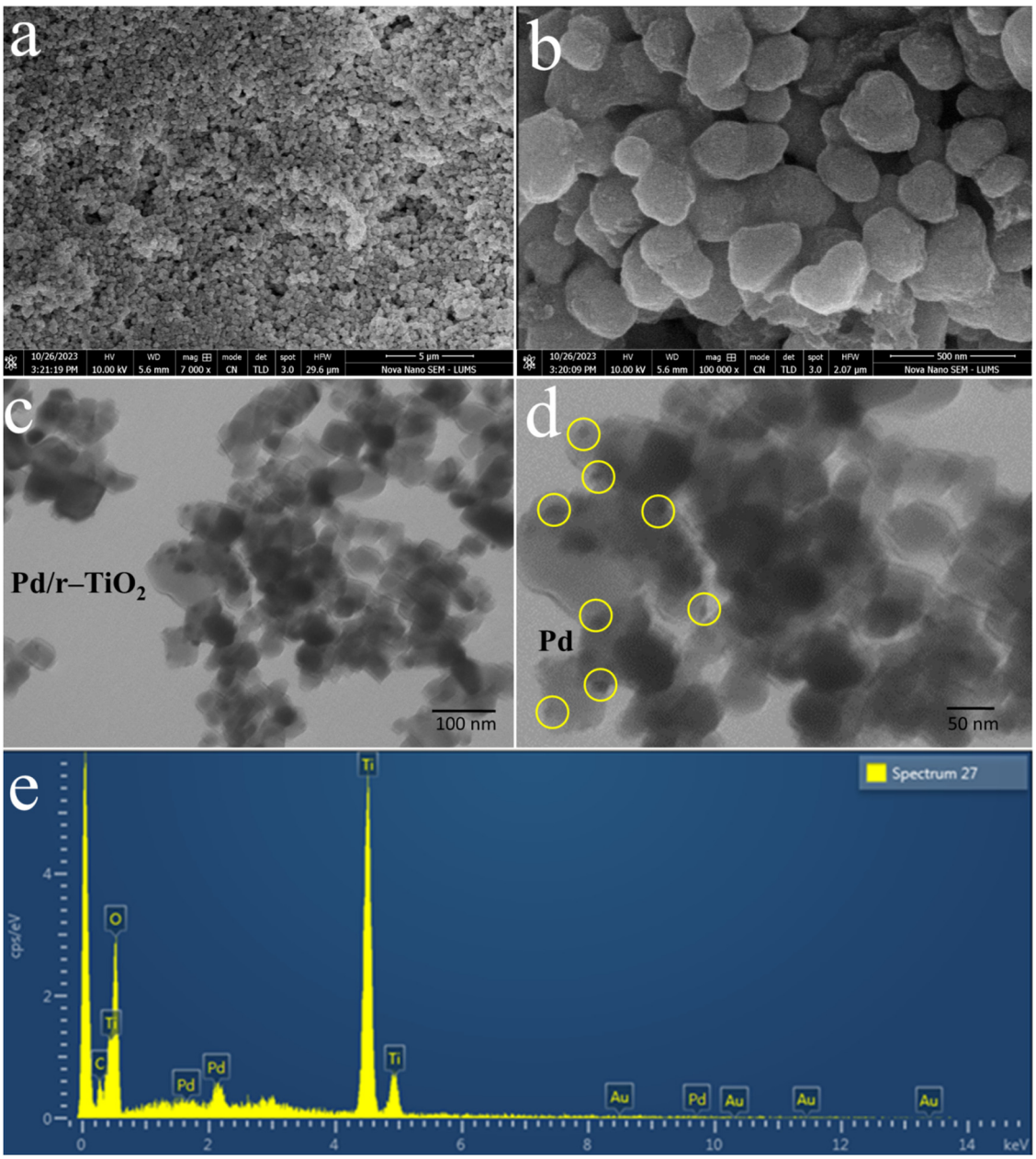

Fig. 3 SEM results (a) 5 μm and (b) 500 nm. (c) TEM results at 100 nm and (d) 50 nm. (e) EDX of Pd/r-TiO_2 catalysts.

analysis also revealed the presence of other elements, such as carbon from the instrument grid and Au from the gold coating.

TEM analysis

TEM results demonstrate the dispersion of Pd nanoparticles over the r-TiO_2 catalyst. As illustrated in Fig. 3(c) and (d), these results indicate a low concentration of Pd particles dispersed on r-TiO_2 surfaces. The presence of low metal contents is attributed to the low metal loading. Thus, it can be seen that Pd nanoparticles are stable and cannot be converted into oxides.[41]

Atomic force microscopy (AFM)

In the current study, atomic force microscopy (AFM) is used to investigate the surface topography, precise sizes and texture morphology of catalysts.[43] The analysis was carried out on an atomic scale, and images of the catalysts are displayed in Fig. 4. The AFM images revealed a uniform distribution of Pd/r-TiO_2 catalyst particles, as presented in the 2D and 3D images in Fig. 4(a), (b) and (d), (e), respectively. The scanning area for the measurement of thickness was 2 × 2 μm, and the catalyst height was 44.8 nm. The average particle size of the catalyst was noted to be 44.5 nm, as shown in Fig. 4c.

UV-Vis/DRS and photoluminescence (PL)

UV-Vis/DRS is a useful technique for examining the optical characteristics of catalysts. In Fig. 5a, the UV-Vis/DRS results of r-TiO_2 and Pd/r-TiO_2 are illustrated. Due to its large band gap (*i.e.*, 3.03 eV), r-TiO_2 exhibits absorption in the ultraviolet

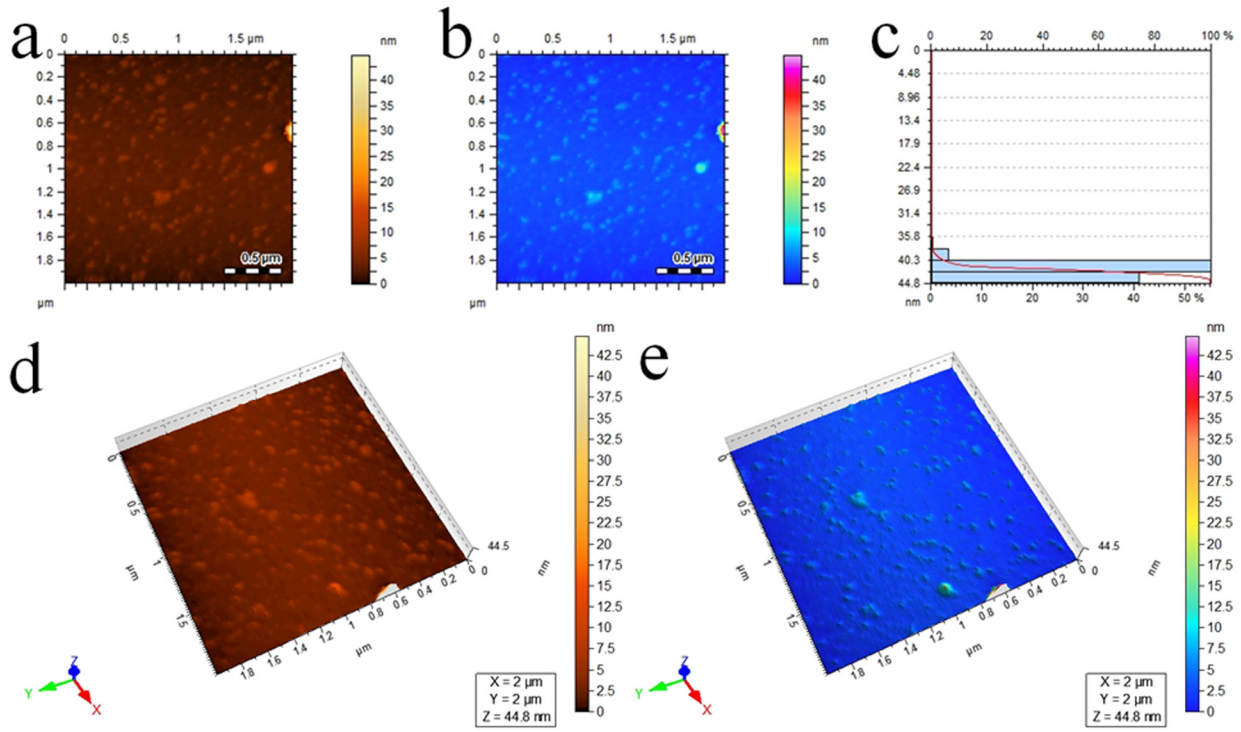

Fig. 4 (a) and (b) 2D AFM images, (c) average height and (d) and (e) 3D AFM images of Pd/r-TiO_2 catalysts.

region.[44] It has been found that Pd metal loaded over the r-TiO_2 surfaces enhances the absorption and affects the band edge. Thus, Pd/r-TiO_2 catalysts exhibit extended absorption (redshift) and exhibit promising absorption in the visible region. Moreover, Pd-cocatalysts exhibit absorption at 545 nm due to the d–d transitions of electrons. The band gap energy diagrams of r-TiO_2 and Pd/r-TiO_2 are illustrated in the inset of Fig. 5a. Pristine r-TiO_2 exhibits a band gap of 3.03 eV, whereas Pd/r-TiO_2 exhibits a reduced band gap, *i.e.*, 2.98 eV.

Photoluminescence reveals insights into the excitations, charge transfer and recombination during the photoreaction.[45] Fig. 5b illustrates the PL emission because of de-excitation in the r-TiO_2 and Pd/r-TiO_2. The results reveal that a back reaction or charge recombination is high in the case of pristine r-TiO_2 due to its overpotential. However, in the case of Pd/r-TiO_2 catalysts, charge recombination is suppressed due to the transfer of electrons to the active sites. Thus, as per synthesis, Pd-cocatalysts enhance the charge transportation and contribute to higher hydrogen generation activities during the photoreactions. Hence, the low intensity of Pd/r-TiO_2 is due to a relatively higher charge transfer. These results support the XRD, Raman and UV-Vis/DRS results.

Electron impedance spectroscopy (EIS)

To assess the charge transfer and charge resistance dynamics, the EIS analysis of pristine r-TiO_2 and Pd/r-TiO_2 was conducted and discussed. In accordance with the PL analysis, the Pd/r-TiO_2 sample has a smaller diameter than r-TiO_2, suggesting a minimal charge transfer resistance and reasonably quick charge transfer kinetics. Fig. 5c displays the EIS results. It is worth mentioning that the presence of Pd-cocatalysts on the r-TiO_2 surfaces accelerates the charge transfer to active sites. Moreover, a higher work function of Pd-cocatalysts suppresses the charge recombination by developing Schottky junctions. These Schottky junctions promote the catalytic performances by rectifying the charges.[46]

BET

The surface area and pore sizes of r-TiO_2 and Pd/r-TiO_2 catalysts were examined by the nitrogen gas adsorption and desorption studies. For both catalysts, the H_1-type hysteresis loop and type-IV isotherm were observed (Fig. 5d). These results indicate the mesoporous nature of the catalysts. On the other hand, using the standard multi-point BET method, the surface area of r-TiO_2 and Pd/r-TiO_2 was determined to be 15.12 $m^2\ g^{-1}$ and 18.26 $m^2\ g^{-1}$, respectively. The inset diagram of Fig. 5d confirmed the narrow pore-size distribution centred at 4.29 nm for both catalysts.

X-ray photon spectroscopy (XPS)

To assess the oxidation states of the constituents and composition of r-TiO_2 and Pd/r-TiO_2 catalysts, the XPS technique was employed.[47] The XPS results are shown in Fig. 6. The survey scan (see Fig. 6a) exhibited all essential elements (*i.e.*, Pd, Ti and O), which are the main constituents of the catalyst. However, carbon was detected as an adventitious element commonly from instrumental grids. XPS results also support the EDX results. Fig. 6b presents the XPS results of Pd metal, with two major peaks appearing at the binding energies of 335.61 eV and 340.91 eV, corresponding to Pd $3d_{5/2}$ and Pd $3d_{3/2}$, respectively.[48] The Ti 2p XPS results were compared for pristine

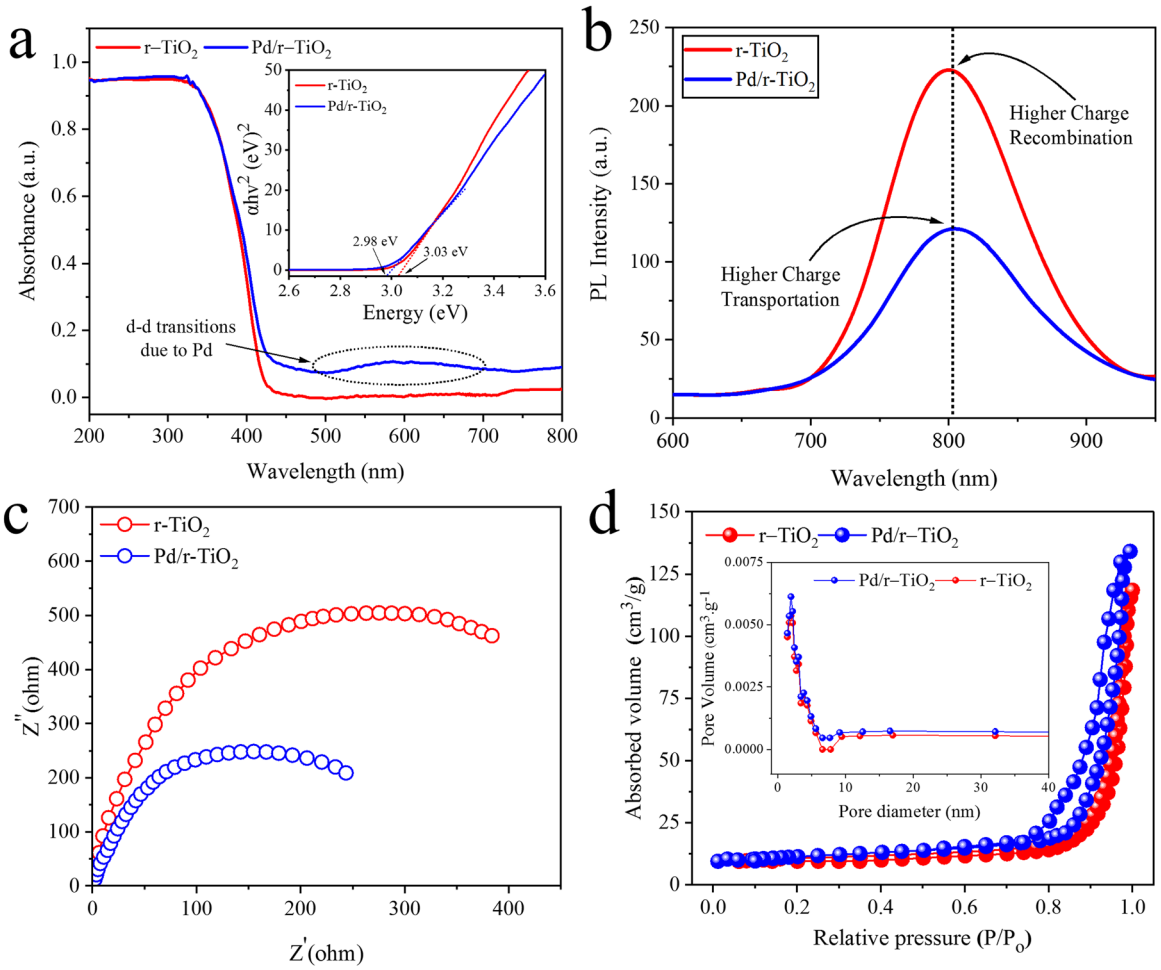

Fig. 5 (a) UV-Vis/DRS results, inset: band gap energy diagrams, (b) PL results, (c) EIS analysis, and (d) BET analysis, inset: pore volume/size distribution of r-TiO_2 and Pd/r-TiO_2.

r-TiO_2 and Pd/r-TiO_2. In the case of pristine r-TiO_2, two Ti peaks appeared at the binding energies of 459.46 eV and 465.16 eV, corresponding to Ti $2p_{3/2}$ and Ti $2p_{1/2}$, respectively.[49] However, after loading Pd over r-TiO_2, a small shift towards higher binding energies was observed, as shown in Fig. 6c. This shift is attributed to the electron transfer between Pd and r-TiO_2. Similarly, two peaks for oxygen appeared at 529.05 eV and 532.25, corresponding to the O^{2-} and –OH of r-TiO_2 structures. However, after the incorporation of Pd, the peaks shifted towards lower binding energies, as shown in Fig. 6d.[50] The binding energies and peak positions of O 1s and Ti 2p slightly changed after Pd deposition. Furthermore, the XPS results of pristine r-TiO_2 or Pd/r-TiO_2 revealed the purity and crystalline morphology that is important for the photoreactions.

Hydrogen generation activities

The photoreactions were carried out in a quartz reactor, and the comparative performances of catalysts are illustrated in Table 1 and Fig. 7. Results revealed that pristine r-TiO_2 delivers 2.15 mmol g^{-1} h^{-1} of hydrogen. This activity is lower than the catalysts having Pd-cocatalysts on r-TiO_2. The significant reason for the lower activity is the overpotential of r-TiO_2 and relatively higher charge recombination. However, catalysts having Pd-cocatalysts over the r-TiO_2 surfaces deliver more hydrogen under similar conditions. Thus, the existence of Pd-cocatalysts on the surfaces of the r-TiO_2 semiconductor creates a Schottky junction at the point of contact between the semiconductor and cocatalysts.[51] The Schottky junctions act as a barrier and stop the back flow of electrons.[52] Moreover, the high metallic character of Pd-cocatalysts makes the semiconductor more conducive to the promotion of electrons to the active centres.[53] For the sake of convenience, a series of catalysts were prepared to optimize the Pd loading onto the r-TiO_2 surfaces. Pd with different ratios, *i.e.*, 0.2, 0.4, 0.6, 0.8 and 1.0 wt%, was deposited on r-TiO_2 and evaluated for catalytic performances. The catalytic performances indicated that $Pd_{0.2}$/r-TiO_2, $Pd_{0.4}$/r-TiO_2, $Pd_{0.6}$/r-TiO_2, $Pd_{0.8}$/r-TiO_2 and $Pd_{1.0}$/r-TiO_2 deliver 6.08, 10.19, 14.12, 19.22 and 23.19 mmol g^{-1} h^{-1} of hydrogen, respectively. It can be clearly seen that the $Pd_{1.0}$/r-TiO_2 catalyst is the most active catalyst of the series that delivers relatively higher hydrogen (*i.e.*, 23.19 mmol g^{-1} h^{-1}) than the other catalysts in this study. Overall, 1.0 wt% loading over the r-TiO_2 surfaces was found to be the optimum; however, increasing the Pd content beyond the optimized ratio was not

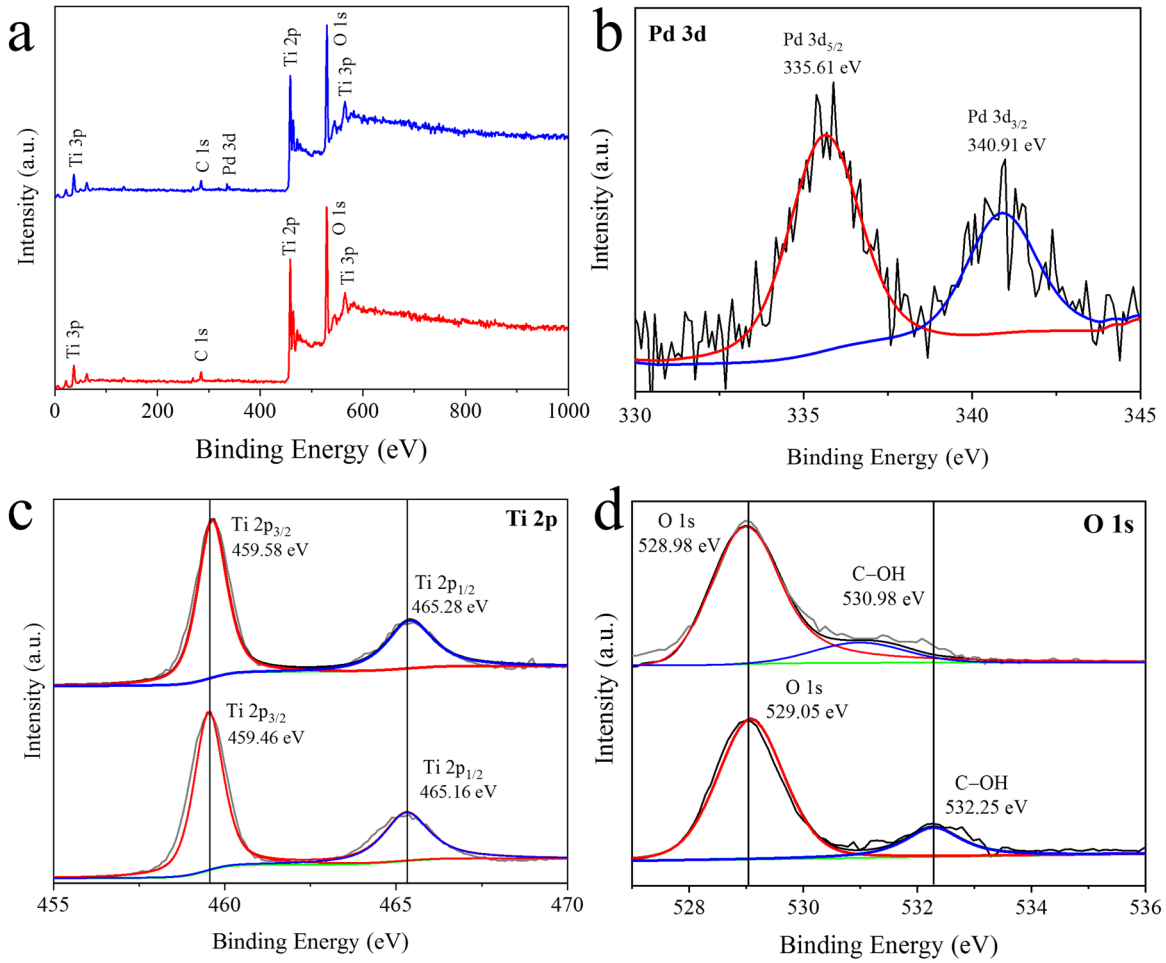

Fig. 6 (a) Survey scans XPS of Pd/r-TiO_2 catalysts. XPS of (b) Pd, (c) Ti and (d) oxygen (O).

Table 1 Comparison of H_2 evolution and optimization Pd wt% on r-TiO_2 surfaces

Sr. no.	Catalysts	Pd/r-TiO_2 ratio (wt%)	Water/ethanol ratio	Photon flux (mW cm^{-2})	Volume[a] M/H	H_2 evolution		QE (%)
						mmol g^{-1}	mmol g^{-1} h^{-1}	
1	Pristine r-TiO_2	0.0 : 100	95 : 5	6.5	30 : 120	12.92	2.15	0.633
2	$Pd_{0.2}$/r-TiO_2	0.2 : 99.80	95 : 5	6.5	30 : 120	36.53	6.08	1.790
3	$Pd_{0.4}$/r-TiO_2	0.4 : 99.60	95 : 5	6.5	30 : 120	61.58	10.19	3.001
4	$Pd_{0.6}$/r-TiO_2	0.6 : 99.40	95 : 5	6.5	30 : 120	84.74	14.12	4.159
5	$Pd_{0.8}$/r-TiO_2	0.8 : 99.20	95 : 5	6.5	30 : 120	115.33	19.22	5.662
6	$Pd_{1.0}$/r-TiO_2	1.0 : 99.00	95 : 5	6.5	30 : 120	139.14	23.19	6.831
7	$Pd_{1.2}$/r-TiO_2	1.2 : 98.80	95 : 5	6.5	30 : 120	145.55	24.25	7.140

[a] Represents the ratio of mixture to headspace volume of the reactor.

very effective for hydrogen generation.[54] This is because the higher metal contents enhance the shadowing effect that blocks the exposure/penetration of photons onto the semiconductor system.[55] Fig. S2 (ESI†) compares the hydrogen generation activities of a Pd/r-TiO_2 catalyst with ethanol and methanol as sacrificial reagents. The results show the relative effectiveness of ethanol and methanol as sacrificial reagents in this catalytic hydrogen production system. It is worth mentioning that using methanol gives slightly higher activities than ethanol.[56] A comparison of the H_2 generation activities of different reported photocatalysts is shown in Table 2.

Mechanism and catalytic reactions

Understanding the photocatalytic water-splitting reaction mechanism is crucial and important for researchers. Fig. 9 illustrates the mechanism of hydrogen evolution on the catalysts reported herein. The water-splitting reaction occurs in three steps: (i) photon absorption by the catalyst particles for

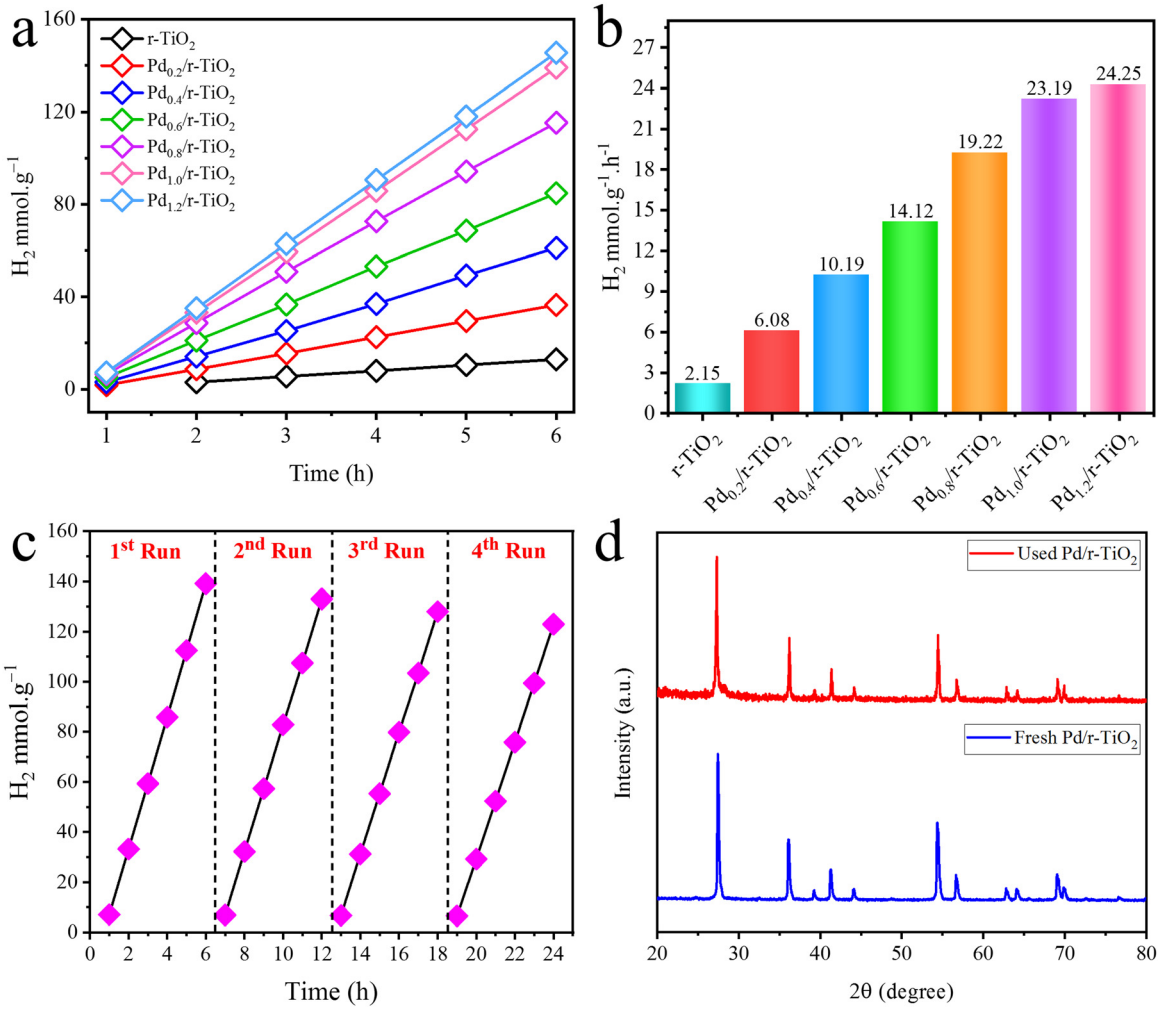

Fig. 7 (a) and (b) H_2 generation activities of catalysts, (c) recyclability test and (d) XRD analysis of used catalysts.

the excitation of electrons, (ii) separation of charges and transfer of these charges to the active sites, and (iii) utilization of charges (electrons/holes) on the redox sites.[66] It is worth mentioning that the bandgap and redox potentials of the catalysts are responsible for the photoreaction.[67] For example, to split water molecules, the oxidation potential of the catalyst must be greater than 1.23 eV, whereas the reduction potential must be lower than the redox potential of hydrogen (0.0 eV).[68] The major drawback associated with r-TiO_2 is its low charge transfer ability due to overpotential. Hence, it cannot control the backflow of electrons to recombine with holes. However, this drawback can be successfully eliminated by the use of cocatalysts with relatively higher work functions (*i.e.*, Pd in this work). Although r-TiO_2 has a 3.03 eV band gap, its band gap can

Table 2 Comparison of H_2 generation activities of catalysts reported in the literature

Catalyst	Light source	Catalyst amount (mg)	Sacrificial reagent	H_2 production (mmol g^{-1} h^{-1})	Ref.
Pd/r-TiO_2	Hg Lamp	7.5	5% Ethanol	23.15	Present study
Au–BaO@TiO_2/CdS	Xe Lamp	10	5% Ethanol	13.54	47
TiO_2/CdS	UV-LED	50	Na_2SO_3	0.051	57
F-TiO_2/CdS	Visible light	5	EDTA	8.342	58
TiO_2@$BaTiO_3$/CdS	Visible light	20	NaH_2PO_2	0.03	59
T-CZS	NIR solar light	10	0.25 M Na_2S/0.35 M Na_2SO_3	0.497	60
ZnS–CdS	300 W Xe lamp	100	0.1 M Na_2SO_3/Na_2S	5.5	61
Ce–ZnCdS	Microwave irradiation	50	0.1 Mol $Na_2S{\cdot}9H_2O$ and Na_2SO_3	2.03	62
$Ti_3C_2T_x$/TiO_2 (P25)	200 W Hg (285–325 nm)	30	25% Methanol	79.5	63
TiO_2/C composite	300 W Xe arc (>420 nm)	50	10 vol% (TEOA)	0.863	64
MXene–TiO_2	300 W xenon	50	10 vol% (TEOA)	390.92	65

be successfully decreased by using Pd-cocatalysts.[69] The Mott Schottky analysis of Pd/r-TiO_2 revealed the CB level at −0.12 eV (Fig. S1, ESI†). The VB level was calculated using eqn (ii)[70] and was found to be 2.91 eV.

$$E_{VB} = E_G - E_{CB} \quad \text{(ii)}$$

Similarly, the light source must be of greater energy than the energy required for the excitation of electrons.[71] When photons fall on the catalyst surface, charge carriers (e^-/h^+) are generated and electrons absorb the energy and are transferred to the conduction band of the semiconductor.[72] It is worth noting that the work function of r-TiO_2 is 4.2 eV, which is lower than that of Pd metal (5.5 eV). Hence, the electrons can easily transfer to the Pd-cocatalysts where they are consumed/utilized for the reduction reaction.[73] The other significant advantage is that the Pd-cocatalysts generate Schottky junctions at the metal/semiconductor interfaces that readily restrict the backflow of electrons.[52] Similarly, due to these Schottky junctions, the flow of electrons to the active sites is easier and rationalized during the photoreaction. On the active sites, the excited electrons are progressively consumed by the aqueous H^+ ions to produce H_2 on the reduction centres. Meanwhile, the sacrificial reagents consume the holes on the semiconductor surfaces.[47,74] Ethanol is oxidized by scavenging the holes and is readily converted into oxidized products (H_2O & CO_2).[75,76] The higher hydrogen generation rates were attributed to the development of the Schottky junctions that suppress charge recombination by rectifying the flow of electrons on the active sites. Excellent metallic characteristics and relatively higher work function of Pd make the steady flow of electrons to be utilized for hydrogen generation.[77]

The scheme that represents the photoreaction for hydrogen evolution reactions is as follows:

$$\text{Pd/r–TiO}_2 + h\nu \rightarrow (\text{VB}) + (\text{CB})e^- \quad \text{(iii)}$$

$$\text{Pd/r–TiO}_2 + H_2O \rightarrow H^+ + OH^- \quad \Delta G^\circ = 237.2 \text{ kJ mol}^{-1} \quad \text{(iv)}$$

$$(\text{CB})2e^- + 2H^+ \rightarrow H_2 \quad E_{CB} = 0.0 \text{ eV} \quad \text{(v)}$$

$$(\text{VB})h^+ + OH^- \rightarrow (OH^\bullet) \quad E_{VB} = 1.23 \text{ eV} \quad \text{(vi)}$$

CB and VB represent the conduction and valence bands, respectively.

Recyclability test

The catalyst stability during photoreaction is an important factor that affects the activity of the catalyst for hydrogen generation.[78] In this work, a recyclability test was conducted to check the stability or reusability of the catalyst. For this purpose, the most active catalyst of the series (Pd/r-TiO_2) was chosen for the recyclability test, and four consecutive runs were performed. It was found that the Pd/r-TiO_2 catalysts exhibit no significant loss in the activity of the catalyst for H_2 generation. Results obtained from the recyclability test revealed that our as-synthesized catalysts are highly stable for the photoreaction, as shown in Fig. 7c. To examine the structural changes in the catalysts after photoreaction, XRD and SEM equipped with elemental maps for Pd/r-TiO_2 catalysts were performed. In the XRD results (see Fig. 7d), no major change was observed, implying that catalysts remain stable after the photoreaction. Fig. 8 illustrates the SEM results with EDX maps of the used Pd/r-TiO_2 catalyst. Fig. 8(a) and (b) reveals the catalyst morphology, showing a rough, textured surface with potential porosity, indicative of a high surface area, and bright, dispersed particles of Pd on the r-TiO_2 support. The EDX maps in Fig. 8(c)–(e) confirm the distribution of Ti, O, and Pd.[79] Pd is distributed

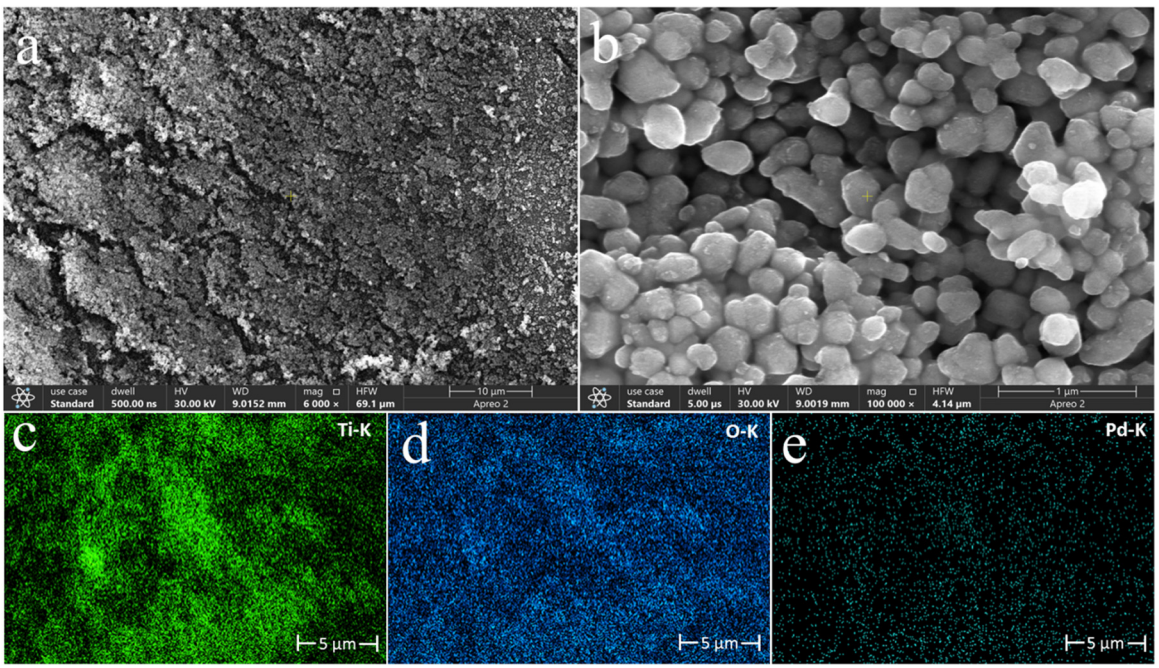

Fig. 8 SEM results of the used Pd/r-TiO_2 catalysts, (a) 10 µm, (b) 1 µm, elementals maps (c) Ti-K (d) O-K and (e) Pd-K.

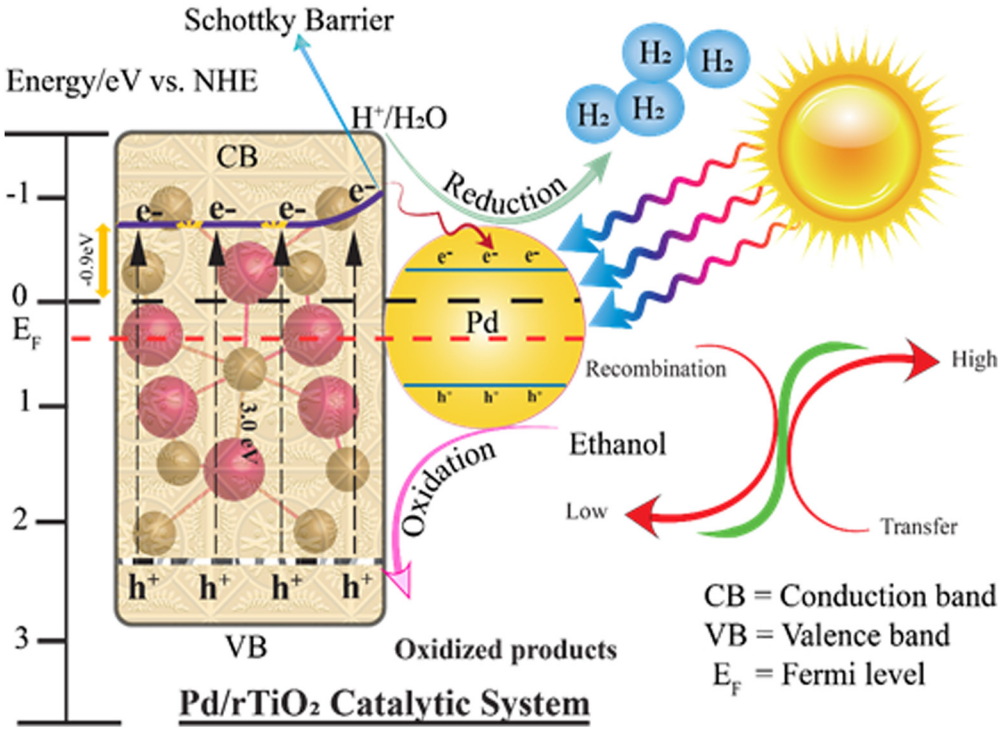

Fig. 9 Mechanism of the water splitting reaction for H_2 generation.

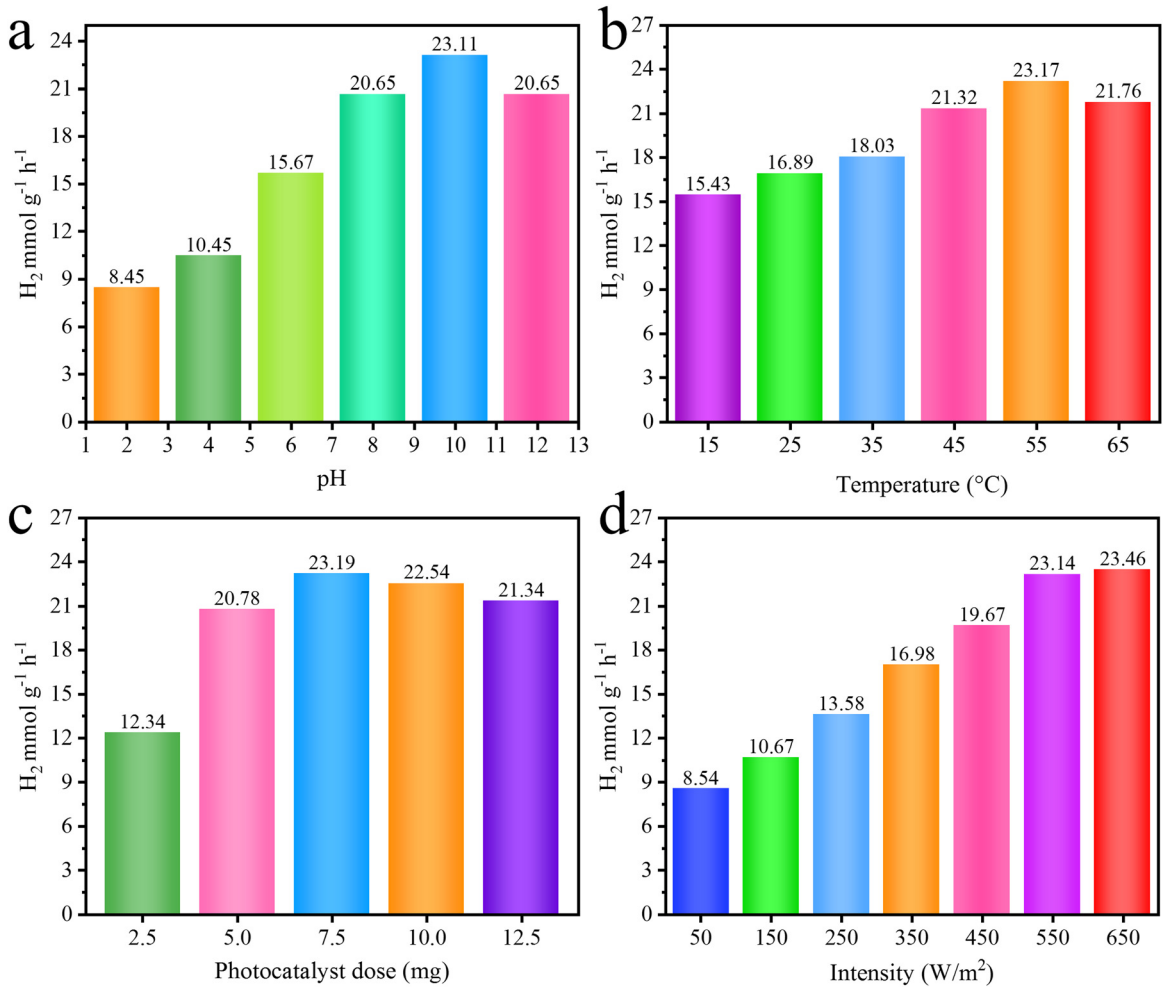

Fig. 10 Effect of (a) pH, (b) temperature, (c) catalyst dose and (d) light intensity on the activity of catalysts.

evenly on the catalysts even after being used four times. Based on these results, Pd is highly dispersed on the r-TiO_2 support, maximizing the active sites for hydrogen production reactions.

Factors affecting the H_2 generation activities

To evaluate the efficiency of the photoreaction (catalytic activities), various factors have been investigated to predict the ideal conditions for hydrogen generation on the most active catalysts, *i.e.*, $Pd_{1.0}$/r-TiO_2. The results obtained for various factors, *i.e.*, pH, temperature, dose of catalysts and intensity of light, are exhibited in Fig. 10a–d, whereas the details and description of these factors are given in the ESI.†

Conclusion

In this study, various catalysts, namely Pd/r-TiO_2 (where Pd = 0.2–1.2%), were prepared and evaluated for hydrogen generation reactions/activities. The deposition of Pd-cocatalysts on the r-TiO_2 surfaces was achieved by chemical reduction and hydrothermal treatments. The morphology, optical characteristics and compositions were examined *via* XRD, FTIR, Raman, UV-Vis/DRS, PL, SEM, TEM, AFM, EDX and XPS analytical approaches. Photoreactions were conducted using the quartz photoreactor MICQ/US-150 mL and a UV lamp (100 W, 360 nm) for the UV source, whereas hydrogen activities were monitored using GC-TCD (Shimadzu/Japan). The results revealed the superior performances of catalysts with Pd-cocatalysts on r-TiO_2 surfaces. To get more insights, various factors, such as the pH, temperature, catalyst dose, and light intensity, were optimized and discussed. It was observed that Pd/r-TiO_2 catalysts deliver 23.19 mmol g^{-1} h^{-1} hydrogen under the optimized conditions, 10 times higher than that of the pristine r-TiO_2. The higher hydrogen generation activities were accredited to the presence of Pd-cocatalysts that restrict charge recombination by developing Schottky junctions. It is worth mentioning that the higher work function of Pd relative to the pristine r-TiO_2 facilitates more electron transfer to the active sites. Thus, higher charge transfer results in more hydrogen evolution efficiencies. Based on the results and catalytic performances, it has been concluded that the ascribed approach holds promise to replace the costly and conventional approaches used for hydrogen production.

Data availability

The data and necessary protocols for this study are included in the ESI.†

Conflicts of interest

There are no conflicts of interest to declare.

Acknowledgements

This study was financially supported by the Higher Education Commission of Pakistan award No. 377/IPFP-II/Batch-I/SRGP/NAHE/HEC/2020/27 and ASIP/R&D HEC/2023/5/22696/124 grants. Experimental work was conducted at the Inorganic Material Laboratory (52s), Institute of Chemistry, The Islamia University of Bahawalpur.

References

1 R. M. Navarro, M. Pena and J. Fierro, *Chem. Rev.*, 2007, **107**, 3952–3991.
2 N. Armaroli and V. Balzani, *Chem. – Eur. J.*, 2016, **22**, 32–57.
3 E. Hussain, I. Majeed, M. A. Nadeem, A. Badshah, Y. Chen, M. A. Nadeem and R. Jin, *J. Phys. Chem. C*, 2016, **120**, 17205–17213.
4 P. Hota, A. Das and D. K. Maiti, *Int. J. Hydrogen Energy*, 2023, **48**, 523–541.
5 J. Nowotny and T. N. Veziroglu, *Int. J. Hydrogen Energy*, 2011, **36**, 13218–13224.
6 L. Preethi, T. Mathews, M. Nand, S. Jha, C. S. Gopinath and S. Dash, *Appl. Catal., B*, 2017, **218**, 9–19.
7 M. Padmini, T. Balaganapathi and P. Thilakan, *Mater. Res. Bull.*, 2021, **144**, 111480.
8 R. Ranjithkumar, P. Lakshmanan, P. Devendran, N. Nallamuthu, S. Sudhahar and M. K. Kumar, *Mater. Sci. Semicond. Process.*, 2021, **121**, 105328.
9 E. Kozlova, A. Rempel', A. Valeeva, T. Gorbunova, N. Kozhevnikova, S. Cherepanova, E. Y. Gerasimov, A. Saraev, E. Y. Korovin and V. Parmon, *Kinet. Catal.*, 2015, **56**, 515–522.
10 L. Biswal, R. Mohanty, S. Nayak and K. Parida, *J. Environ. Chem. Eng.*, 2022, **10**, 107211.
11 H. Yu, P. Xiao, J. Tian, F. Wang and J. Yu, *ACS Appl. Mater. Interfaces*, 2016, **8**, 29470–29477.
12 M. E. Aguirre, R. Zhou, A. J. Eugene, M. I. Guzman and M. A. Grela, *Appl. Catal., B*, 2017, **217**, 485–493.
13 M. Z. Abid, K. Rafiq, A. Rauf and E. Hussain, *Nanoscale Adv.*, 2024, **6**, 5861–5873.
14 R. Lu, X. Xu, J. Chang, Y. Zhu, S. Xu and F. Zhang, *Appl. Catal., B*, 2012, **111**, 389–396.
15 H. Huang, Y.-X. Li, G.-J. Jiang, H.-L. Wang and W.-F. Jiang, *Inorg. Chem.*, 2021, **60**, 17325–17338.
16 M. Jalil, K. Rafiq, M. Z. Abid, A. Rauf, S. Wang, S. Iqbal and E. Hussain, *Nanoscale Adv.*, 2023, **5**, 3233–3246.
17 F. Saleem, M. Z. Abid, K. Rafiq, A. Rauf, K. Ahmad, S. Iqbal, R. Jin and E. Hussain, *Int. J. Hydrogen Energy*, 2023, **52**, 305–319.
18 M. Jalil, K. Rafiq, M. Z. Abid, M. Rafay, A. Rauf, R. Jin and E. Hussain, *Catal. Sci. Technol.*, 2024, **14**, 850–862.
19 A. Nasir, S. Khalid, T. Yasin and A. Mazare, *Energies*, 2022, **15**, 6248.
20 T. Haq, M. Pasha, Y. Tong, S. A. Mansour and Y. Haik, *Appl. Catal., B*, 2022, **301**, 120836.
21 W. Li, X.-s Chu, F. Wang, Y.-y Dang, X.-y Liu, T.-h Ma, J.-y Li and C.-y Wang, *Appl. Catal., B*, 2022, **304**, 121000.

22 J. Huo, P. Duan, H. N. Pham, Y. J. Chan, A. K. Datye, K. Schmidt-Rohr and B. H. Shanks, *Catal. Sci. Technol.*, 2018, **8**, 3548–3561.
23 Ş. Sungur, *Handbook of nanomaterials and nanocomposites for energy and environmental applications*, 2021, pp. 713–730.
24 Q. Mao, D. Zeng, K. Xu and C. Xie, *RSC Adv.*, 2014, **4**, 58101–58107.
25 L. E. Oi, M.-Y. Choo, H. V. Lee, H. C. Ong, S. B. Abd Hamid and J. C. Juan, *RSC Adv.*, 2016, **6**, 108741–108754.
26 E. Hussain, M. Jalil, M. Z. Abid, J. Mansab, R. H. Althomali, S. Wang, A. Rauf and K. Rafiq, *Mater. Adv.*, 2024, **5**, 6572–6585.
27 A. Ishaq, K. Rafiq, M. Z. Abid, U. Aiman and E. Hussain, *Renewable Energy*, 2024, **237**, 121817.
28 T. Ishaq, M. Yousaf, I. A. Bhatti, A. Batool, M. A. Asghar, M. Mohsin and M. Ahmad, *Int. J. Hydrogen Energy*, 2021, **46**, 39036–39057.
29 A. J. Cowan and J. R. Durrant, *Chem. Soc. Rev.*, 2013, **42**, 2281–2293.
30 Y. Liu, J. Guo, E. Zhu, L. Liao, S.-J. Lee, M. Ding, I. Shakir, V. Gambin, Y. Huang and X. Duan, *Nature*, 2018, **557**, 696–700.
31 X. Tang, A. Yu, Q. Yang, H. Yuan, Z. Wang, J. Xie, L. Zhou, Y. Guo, D. Ma and S. Dai, *J. Am. Chem. Soc.*, 2024, **146**, 3764–3772.
32 Z. Khan, T. R. Chetia, A. K. Vardhaman, D. Barpuzary, C. V. Sastri and M. Qureshi, *RSC Adv.*, 2012, **2**, 12122–12128.
33 M. Hazarika, P. K. Boruah, M. Pal, M. R. Das and C. Tamuly, *ChemistrySelect*, 2019, **4**, 1244–1250.
34 M. Z. Abid, A. Ilyas, K. Rafiq, A. Rauf, M. A. Nadeem, A. Waseem and E. Hussain, *Environ. Sci.: Water Res. Technol.*, 2023, **9**, 2238–2252.
35 C. Rani, D. K. Pathak, M. Tanwar, S. Kandpal, T. Ghosh, M. Y. Maximov and R. Kumar, *Mater. Adv.*, 2022, **3**, 1602–1608.
36 E. Hussain, S. Khan, M. Jalil, M. Z. Abid, A. Rauf, N. N. Riaz, A. Hashem, A. Kumar, E. F. Abd_Allah and K. Rafiq, *Fuel*, 2025, **382**, 133672.
37 R. Panigrahi and S. K. Srivastava, *RSC Adv.*, 2014, **4**, 53055–53059.
38 M. Z. Abid, K. Rafiq, A. Rauf, S. S. Ahmad Shah, R. Jin and E. Hussain, *Nanoscale Adv.*, 2023, **5**, 3247–3259.
39 O. A. Baturina, S. R. Aubuchon and K. J. Wynne, *Chem. Mater.*, 2006, **18**, 1498–1504.
40 A. Skreiberg, Ø. Skreiberg, J. Sandquist and L. Sørum, *Fuel*, 2011, **90**, 2182–2197.
41 M. Z. Abid, K. Rafiq, A. Rauf, R. H. Althomali and E. Hussain, *Mater. Adv.*, 2024, **5**, 2238–2252.
42 S. C. Mali, A. Dhaka, C. K. Githala and R. Trivedi, *Biotechnol. Rep.*, 2020, **27**, e00518.
43 M. R. Nellist, F. A. Laskowski, J. Qiu, H. Hajibabaei, K. Sivula, T. W. Hamann and S. W. Boettcher, *Nat. Energy*, 2018, **3**, 46–52.
44 H. Tang, S. Chang, K. Wu, G. Tang, Y. Fu, Q. Liu and X. Yang, *RSC Adv.*, 2016, **6**, 63117–63130.
45 Y. Ma, T.-W. Choi, S. H. Cheung, Y. Cheng, X. Xu, Y.-M. Xie, H.-W. Li, M. Li, H. Luo and W. Zhang, *Nanoscale*, 2019, **11**, 8736–8743.
46 A. Ter Heijne, O. Schaetzle, S. Gimenez, F. Fabregat-Santiago, J. Bisquert, D. P. Strik, F. Barriere, C. J. Buisman and H. V. Hamelers, *Energy Environ. Sci.*, 2011, **4**, 5035–5043.
47 M. Sabir, K. Rafiq, M. Z. Abid, U. Quyyum, S. S. A. Shah, M. Faizan, A. Rauf, S. Iqbal and E. Hussain, *Fuel*, 2023, **353**, 129196.
48 K. Rafiq, K. U. Sahar, M. Z. Abid, S. Attique, U. U. Rehman, A. Rauf and E. Hussain, *Energy Adv.*, 2024, **3**, 983–996.
49 M. Z. Abid, K. Rafiq, A. K. Buzdar, M. Z. Waleed and E. Hussain, *J. Cleaner Prod.*, 2025, **490**, 144680.
50 L. Wang, Y. Lin, W. Guo, Y. Yang, R. Zhang, Y. Zhai and Y. Liu, *New J. Chem.*, 2021, **45**, 14458–14468.
51 X.-H. Li and M. Antonietti, *Chem. Soc. Rev.*, 2013, **42**, 6593–6604.
52 T. Shan, L. Luo, T. Chen, L. Deng, M. Li, X. Yang, L. Shen and M.-Q. Yang, *Green Chem.*, 2023, **25**, 2745–2756.
53 Z. Liang, B. Sun, X. Xu, H. Cui and J. Tian, *Nanoscale*, 2019, **11**, 12266–12274.
54 E. Hussain, M. Idrees, M. Jalil, M. Z. Abid, K. Aljohani and K. Rafiq, *Nanoscale*, 2025, **17**, 3436–3450.
55 B. A. Pinaud, J. D. Benck, L. C. Seitz, A. J. Forman, Z. Chen, T. G. Deutsch, B. D. James, K. N. Baum, G. N. Baum and S. Ardo, *Energy Environ. Sci.*, 2013, **6**, 1983–2002.
56 F. Guzman, S. S. Chuang and C. Yang, *Ind. Eng. Chem. Res.*, 2013, **52**, 61–65.
57 A. Meng, B. Zhu, B. Zhong, L. Zhang and B. Cheng, *Appl. Surf. Sci.*, 2017, **422**, 518–527.
58 K. Dai, J. Lv, J. Zhang, G. Zhu, L. Geng and C. Liang, *ACS Sustainable Chem. Eng.*, 2018, **6**, 12817–12826.
59 C. Yang, Y. Chen, T. Chen, S. Rajendran, Z. Zeng, J. Qin and X. Zhang, *Fuel*, 2022, **314**, 122758.
60 H. Zhao, H. Liu, L. Guo, C. Xing and X. Li, *Int. J. Hydrogen Energy*, 2019, **44**, 24559–24571.
61 J. Xu, *Int. J. Electrochem. Sci.*, 2017, **12**, 2253–2261.
62 Y. Wang, H. Jin, Y. Li, J. Fang and C. Chen, *Int. J. Hydrogen Energy*, 2022, **47**, 962–970.
63 T. Su, Z. D. Hood, M. Naguib, L. Bai, S. Luo, C. M. Rouleau, I. N. Ivanov, H. Ji, Z. Qin and Z. Wu, *ACS Appl. Energy Mater.*, 2019, **2**, 4640–4651.
64 J. Wang, Y. Shen, S. Liu and Y. Zhang, *Appl. Catal., B*, 2020, **270**, 118885.
65 S. Zong, J. Liu, Z. Huang, L. Liu, J. Liu, J. Zheng and Y. Fang, *J. Alloys Compd.*, 2022, **896**, 163039.
66 Q. Wang and K. Domen, *Chem. Rev.*, 2019, **120**, 919–985.
67 S. Hu, F. Li, Z. Fan, F. Wang, Y. Zhao and Z. Lv, *Dalton Trans.*, 2015, **44**, 1084–1092.
68 D. Singh, S. K. Gupta, Y. Sonvane, A. Kumar and R. Ahuja, *Catal. Sci. Technol.*, 2016, **6**, 6605–6614.
69 K. Rafiq, K. U. Sahar, M. Z. Abid, S. Attique, U. Rehman, A. Rauf and E. Hussain, *Energy Adv.*, 2024, **3**, 983–996.
70 M. Z. Abid, K. Rafiq, A. Rauf, R. H. Althomali, R. Jin and E. Hussain, *Renewable Energy*, 2024, **225**, 120223.
71 J. W. Lichtman and J.-A. Conchello, *Nat. Methods*, 2005, **2**, 910–919.
72 P. R. Chowdhury and K. G. Bhattacharyya, *RSC Adv.*, 2015, **5**, 92189–92206.

73 S. N. Habisreutinger, L. Schmidt-Mende and J. K. Stolarczyk, *Angew. Chem., Int. Ed.*, 2013, **52**, 7372–7408.
74 C. Joyce-Pruden, J. K. Pross and Y. Li, *J. Org. Chem.*, 1992, **57**, 5087–5091.
75 K. U. Sahar, K. Rafiq, M. Z. Abid, A. Rauf, U. Rehman, M. A. Nadeem, R. Jin and E. Hussain, *Colloids Surf., A*, 2023, **674**, 131942.
76 M. Wang, J. Ioccozia, L. Sun, C. Lin and Z. Lin, *Energy Environ. Sci.*, 2014, **7**, 2182–2202.
77 S. Sarkar and S. C. Peter, *Inorg. Chem. Front.*, 2018, **5**, 2060–2080.
78 K. A. Connelly and H. Idriss, *Green Chem.*, 2012, **14**, 260–280.
79 S. Jung, N. Reed, G. Yablonsky and P. Biswas, *Catal. Sci. Technol.*, 2021, **11**, 4763–4775.